Fuel 350 (2023) 128825

Contents lists available at ScienceDirect

Fuel

journal homepage: www.elsevier.com/locate/fuel

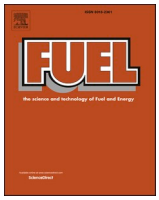

Full Length Article

Effects of ammonia on combustion of coal in stoichiometric premixed methane–air flames

Yueh-Heng Li [a,b,*], Bo-Cheng Chuang [a], Po-Hung Lin [a], Janusz Lasek [c]

[a] Department of Aeronautics and Astronautics, National Cheng Kung University, Tainan 70101, Taiwan
[b] International Doctoral Degree Program on Energy Engineering, National Cheng Kung University, Tainan 70101, Taiwan
[c] Institute of Energy and Fuel Processing Technology, Zabrze 41-803, Poland

ARTICLE INFO

Keywords:
Ammonia
Coal combustion
Two-color pyrometry
Hybrid flames

ABSTRACT

NH_3 has long been considered a promising alternative fuel·NH_3 from renewables can be used for energy storage·NH_3 is a zero-carbon molecule and can be burned directly and used as a hydrogen carrier. Compared with hydrocarbon fuels, NH_3 has several drawbacks, such as an inferior flammability limit, flame temperature, and flame burning velocity, resulting in a lower reactivity rate and the production of pollutants.

Therefore, cofiring coal with NH_3 is an approach that has been growing in popularity. This study investigated the combustion of coal cofired with NH_3 and conducted two-color pyrometry to measure the temperature profiles of coal particles in hybrid flames, that is, methane–coal–air and methane–NH_3–coal–air premixed flames. The axial temperature distribution at the center of the flame was measured using two-color pyrometry and a thermocouple. The temperature values obtained were not identical but exhibited similar trends. The results indicated that the temperature at the origin significantly decreased upon ammonia addition, but as the measuring height increased, the final temperatures approached similarity.

In addition, the emissions of pollutants such as CO and NOx were also measured. The results indicate that the addition of coal particles without ammonia gas leads to an increase in CO concentration due to the pyrolysis of the pulverized coal. However, there was no significant impact on NOx emissions.

In contrast, the addition of coal particles under $CH_4 - NH_3$ gas combustion conditions results in a significant decrease in both CO and NOx concentrations. Specifically, under the 80 %CH_4 + 20 %NH_3 condition and with a coal particle feeding rate increasing from 0 to 0.24 g/min, there was a reduction of approximately 34% in CO concentration and 35% in NOx concentration.

In order to confirm the coal consumption rate, coal particles were captured before and after flame sheet using a metal grid, and the particle projected area was determined based on scanning electron microscopy (SEM) images. These results provided evidence that the addition of NH_3 to the CH_4 – air flame enhances coal combustion, as indicated by a decrease in the particle shrinkage rate and sampling density.

1. Introduction

Coal is the most abundant hydrocarbon fuel. A substantial amount of energy needs are met using coal, especially in developing nations [1]. Hydrocarbon fuels contribute to climate change and cause air pollution and global warming. Carbon emissions must thus be reduced to zero [2] by means of burning alternative fuels [36,41,43] or enhancing combustion efficiency [35,44]. Fossil fuels have been widely used in industry and transportation since the industrial revolution [3,4]. The World Health Organization has suggested that pollutants—such as particulate matter, volatile organic compounds, nitrogen oxides (NO_X), and sulfur dioxide—are harmful to humans [42]. Fine, suspended particles are easily absorbed into human lungs and can negatively affect health [5,37,39,40].

Pulverization of coal is a common method of preparing coal for burning. Coal has a high heating value (approximately 17.4–23.9 MJ/kg) and excellent energy density and can be obtained easily. The utilization of coal, such as combustion or gasification, involves intricate chemical reactions such as devolatilization and volatiles oxidation [6,7]. Quintessentially, devolatilization is critical for solid fuel combustion, and persistently occurs during the life span of coal particles. According to Jianglong *et al.* [8], char is structurally complex and highly

* Corresponding author at: Department of Aeronautics and Astronautics, National Cheng Kung University, Tainan 70101, Taiwan.
E-mail address: yueheng@mail.ncku.edu.tw (Y.-H. Li).

https://doi.org/10.1016/j.fuel.2023.128825
Received 25 March 2023; Received in revised form 10 May 2023; Accepted 28 May 2023
Available online 3 June 2023

heterogeneous both within and among particles. Various factors, such as pressure and heating rate, affect the chemical characteristics of char. Temperature affects the structure of char [9]. The behavior of coal during combustion and gasification varies considerably depending on the composition of the coal particles. The structure of char strongly influences the reactions it undergoes and the ash that then forms [10–13]. Essenhigh *et al.* [14] described the relation between heating rate and particle size as leading to three possible situations: heterogeneous ignition, homogeneous ignition, or hetero-homogeneous joint ignition (the homogeneous and heterogeneous ignitions occur at the same time). Adeosun *et al.* [15] investigated the effect of particle size on ignition delay and found that coal particles with a diameter of 90–124 μm ignited more quickly than those with a diameter of 75–89 μm [16,17]. Furthermore, they also indicated that the particle size which below 90 mm is oxygen-dependent and above 90 mm is temperature-dependent. It leads to homogeneows ignition of coal strems.

Ammonia (NH_3) has long been considered a promising alternative fuel, a source of energy, and a heating component. The use of NH_3 for fuel has been gaining attention recently·NH_3 from renewables can be used for energy storage·NH_3 is a zero-carbon molecule and can be burned directly and used as a hydrogen carrier. The range of applications of NH_3 is rapidly expanding. Because NH_3 is composed of nitrogen and hydrogen, it can easily be stored, and this makes it a versatile, convenient medium·NH_3 produces NO_X at a high rate and has low reactivity. This presents a significant challenge to its direct utilization as a fuel [18]·NH_3 has a lower flammability limit, flame temperature, and flame burning velocity than do hydrocarbon fuels [45]. Thus, it is interesting to know the combustion behavior of coal when methane (CH_4) was partially replaced by NH_3. The cofiring of a CH_4–NH_3–air mixture produced flames with an expanding spherical plume [19]. A CH_4–NH_3–air flame was discovered to release less CO_2, propagate more slowly, and be thicker than a pure CH_4–air flame [19]. Reduction of NO_X dominated the reaction, with the flame temperature being decreased when the ratio of NH_3 was increased. Cofiring coal with NH_3 has been proposed as an approach for coal phasedown and to reduce carbon emissions.

A nonintrusive system of flame temperature measurement, two-color pyrometry, is interpreted by H. Zhao et al. The principle of two-color pyrometry is that two alternative wavelengths of thermal radiation are captured, and the true flame temperature can be determined mathematically by applying Planck's equation [20,21].

This study investigates the effect of ammonia replacement on coal combustion and incorporates two-color pyrometry. It examines the variations in flame temperature distribution with different proportions of ammonia substitution and different coal feed rates. Additionally, it compares the temperature distribution errors under different wavelength combinations and identifies the optimal combination.

It should be noted that this study utilizes a precision aerosol generator for transporting pulverized coal. The equipment has a maximum allowable coal particle concentration of 67.58 g/m^3. As a result, four experimental points were evenly distributed between 0 and the maximum value to conduct the experiments. In terms of ammonia replacement, the primary objective was to substitute a portion of the fuel and investigate the co-combustion scenario. To ensure a balanced focus on both ammonia and co-combustion conditions, a maximum replacement proportion of 20% was carefully selected for the subsequent experiments.

The objective of this study is to observe the combustion behavior of pulverized coal combined with NH_3. In addition to two-color pyrometry, further investigation was conducted on the variations of pollutants under different combustion conditions. In the end of this study, the analysis was ultimately confirmed through scanning electron microscopy (SEM) images, which demonstrated that the addition of ammonia gas enhances the consumption rate of coal.

2. Theory underlying two-color pyrometry

According to the thermal equilibrium model, the flame and soot temperatures should be approximately the same [21]. An equation for calculating the temperature of the surface of soot particles by using two-color pyrometry has been proposed [22]. According to Planck's law, the black body spectral radiance $I_{b,\lambda}$ depends on the wavelength λ and temperature T:

$$I_{b,\lambda}(T) = \frac{C_1}{\lambda^5\left[exp\left(\frac{C_2}{\lambda T}\right) - 1\right]} \tag{1}$$

where $I_{b,\lambda}$ is the emission of a monochromatic black body (W/m^3); λ is the wavelength (nm), T is the temperature (K); C_1 is a constant based on Planck's first law, with $C_1 = 3.7418 \times 10^{-13}$ Wm^2; and C_2 is a constant based on Planck's second law, with $C_2 = 1.4388 \times 10^{-2}$ mK.

The monochromatic emissivity of a nonblack body can be expressed as follows:

$$\varepsilon_\lambda = \frac{I_\lambda(T)}{I_{b,\lambda}(T)} \tag{2}$$

where ε_λ is the ratio of the black body radiation emitted by the surface of the nonblack body at wavelength λ, $I_\lambda(T)$ is the emission power of a monochromatic nonblack body (W/m^3), and $I_{b,\lambda}(T)$ is the emission power of a monochromatic black body (W/m^3).

In two-color pyrometry, an apparent temperature T_a is introduced and assumed to be the temperature at which a black body emits the same amount of radiation as a nonblack body at the same temperature. T_a, also known as the brightness temperature, is defined as follows:

$$I_{b,\lambda}(T_a) = I_\lambda(T) \tag{3}$$

The apparent temperature and monochromatic emissivity equation can be further rewritten as follows:

$$\varepsilon_\lambda = \frac{I_{b,\lambda}(T_a)}{I_{b,\lambda}(T)} \tag{4}$$

By applying Planck's law, the emissivity equation can be further rewritten as follows:

$$\varepsilon_\lambda = \frac{\left[exp\left(\frac{C_2}{\lambda T}\right) - 1\right]}{\left[exp\left(\frac{C_2}{\lambda T_a}\right) - 1\right]} \tag{5}$$

Hottel et al. [20] proposed the following empirical relationship equation for the emissivity of soot particles:

$$\varepsilon_\lambda = 1 - exp\left(\frac{-KL}{\lambda^\alpha}\right) \tag{6}$$

where K is an absorption coefficient and a function of the soot particle density ($m^{\alpha-1}$) and L is the flame's geometric thickness measured along the optical axis of the detection system (m).

On the basis of the values selected for parameter α, the soot temperature can be estimated. Parameter α is a function of the optical and physical properties of the soot in the flame. The type of fuel can also affect the value of α. Zhao et al. [21] suggested that the value of α is not crucial for calculating flame temperature when two wavelengths in the visible region are selected. Matsui et al. [23] found that the correlation between emission and wavelength was rationalized at $\alpha = 1.39$ within the visible range. Furthermore, they recommended a wavelength range of 500–750 nm.

Equations (5) and (6) can be combined as follows:

$$KL = -\lambda^\alpha ln\left[1 - \left(\frac{exp\left(\frac{C_2}{\lambda T}\right) - 1}{exp\left(\frac{C_2}{\lambda T_a}\right) - 1}\right)\right] \tag{7}$$

The purpose is to determine the temperature; therefore, unknown factors must be eliminated. The concept of equality can be utilized to eliminate unknown factors. Thermal radiation of two wavelengths is detected simultaneously, and the ratio between this different-wavelength radiation determines the flame temperature. By inputting the different wavelengths to equation (7), the unknown factor *KL* can be obtained. Therefore, the equation can be further rewritten as follows:

$$ln\left[1-\left(\frac{exp\left(\frac{C_2}{\lambda_1 T}\right)-1}{exp\left(\frac{C_2}{\lambda_1 T_{a1}}\right)-1}\right)\right]^{\lambda_1{}^{\alpha_1}} = ln\left[1-\left(\frac{exp\left(\frac{C_2}{\lambda_2 T}\right)-1}{exp\left(\frac{C_2}{\lambda_2 T_{a2}}\right)-1}\right)\right]^{\lambda_2{}^{\alpha_2}} \quad (8)$$

where T_{a1} and T_{a2} are the apparent temperatures corresponding to wavelengths λ_1 and λ_2, respectively. The flame temperature T can be determined using equation (8) if the apparent flame temperatures T_{a1} and T_{a2} are known. A calibration system for two-color optical pyrometry can measure the two apparent flame temperatures at these wavelengths.

The unknown factor (*KL*) can be eliminated by rearranging the equation for two different wavelengths. By measuring the flame at two wavelengths (λ_1 and λ_2), the apparent temperatures T_{a1} and T_{a2} can be determined instantaneously, enabling calculation of the flame temperature. The choice of wavelength λ_1 and λ_2 is discussed later. The soot temperature T_{soot} was calculated using equation (8) in this study. Due to its nonintrusive nature, two-color pyrometry may be inaccurate. Therefore, different wavelength filters were evaluated to determine the optical path length and assess the temperature distribution.

A schematic of the imaging system is displayed in Fig. 1. The system consisted of a furnace, an objective target, a group of different wavelength filters (in general, narrow-band pass filters are used), two prisms (also called beam splitters), a lens, and a charge-coupled device (CCD, PCO AG, Kelheim, Germany). To obtain two individual images, double monochromatic signals were acquired using twin prisms simultaneously during photographing. Narrow-band pass filters were placed in front of the dual-prism assembly to enable selection of the band to pass; the filter was changed on the basis of the working principle to refract the target image into two identical images. The prisms had 4-mm sides and were shaped like isosceles triangles. Shawn et al. [24] recommended that objective targets be placed far from a CCD camera to improve accuracy and decrease the parallax angle, although doing so may sacrifice overall spatial resolution and signal strength.

By adjusting the arrangement of the dual prism, the deviation angle was minimized and approximately parallel beams of light were obtained. Due to the target being far from the CCD camera, zoom lenses with long focal lenses were used to improve the resolution. To obtain the optimal results, the exposure time was set to 1 ms and image resolution was set to 1392 × 1040 pixels; the pixel binning was fixed.

3. Experimental apparatus

The slot burner was 40-mm long and 4-mm wide. The wall of the stainless steel burner was 2-mm thick. Every plane had an inner surface polished through milling performed with computer numerical control. Bradley and Mathew [25] suggested that an increase in the length-to-width ratio reduces the end-effect errors of rectangular burners. The burner was 146-mm tall. Inside the burner, a 40-mm-wide honeycomb and a stainless steel mesh screen were used to straighten the flow field to suit the mixing fluid. One square inch of 100 mesh of honeycomb and stainless steel mesh was used. Fig. 2**(a)** shows how the flow was rectified, and Fig. 2**(b) and (c)** show the device in more detail. The honeycomb prevented the flame from flashing back into the combustor. The outside of the burner is sloped irregularly to accelerate the fluid away from the burner. Another inlet port was the port through which the coal particles entered. The coal particles were blocked by the honeycomb and stainless steel mesh; therefore, the inlet channels had to be separated.

The CH_4 and NH_3 used in this study had a purity of 99.9% and were stored in a highly pressurized tank. Dry air (79 % N_2 and 21% O_2) was provided by a high-pressure pump. An electronic mass flow controller was used to control the volume of gas. All the conditions of the equivalent ratio were fixed at a stoichiometric value. In the idealized reaction depicted below, a stoichiometric mixture of CH_4–NH_3–air was calculated by Rocha et al. [26].

$$(1-x_{NH_3})CH_4 + x_{NH_3}NH_3 + \left(2-\frac{5x_{NH_3}}{4}\right)(O_2+3.76N_2) \rightarrow (1-x_{NH_3})CO_2 + \left(2-\frac{x_{NH_3}}{2}\right)H_2O + (7.52-4.2x_{NH_3})N_2 \quad (9)$$

where x_{NH_3} is the molar fraction of the fuel mixture, calculated as follows:

$$x_{NH_3} = \frac{v_{NH_3}}{v_{NH_3}+v_{CH_4}} \quad (10)$$

where v_{NH_3} and v_{CH_4} are the mass flow velocities of NH_3 and CH_4, respectively.

Table 1 shows the volume flow rate under each condition for flames cofired with CH_4 − NH_3 − air at stoichiometric values and an overall flow rate of 1 m/s. The flame structure was captured using a digital single-lens reflection camera (D80, NIKON, Japan). A digital camera with a Sigma macro lens (105 mm F/2.8 EX DG OS HSM, for Nikon F tube) was used. The camera was set to an ISO of 100, its exposure time was set to 0.04 s (1/25 s^{-1}), its aperture was set to F3.5, and its control

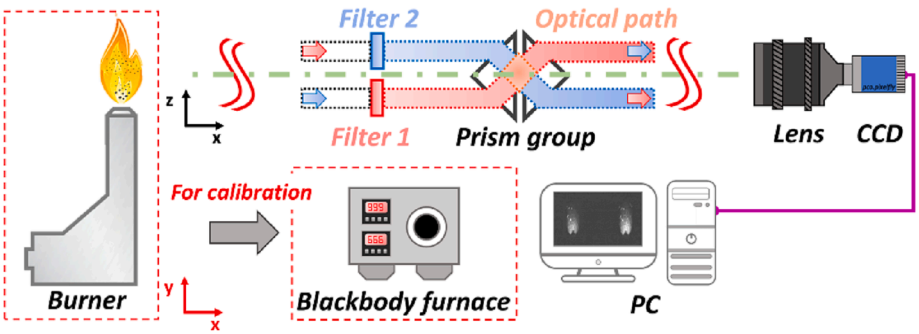

Fig. 1. Imaging system.

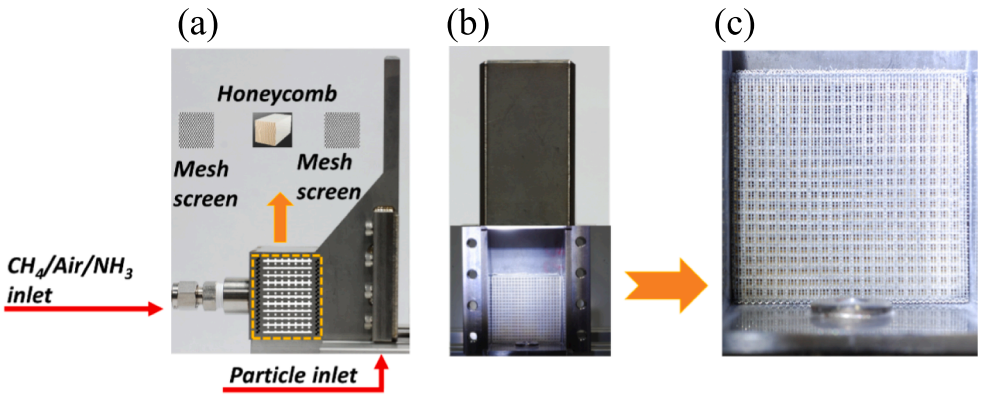

Fig. 2. Interior of the slot burner.

Table 1
Volume flow rate under each condition.

	CH_4 [l/min]	Air [l/min]	NH_3 [l/min]
100% CH_4 + 0% NH_3	0.91	8.68	0
90% CH_4 + 10% NH_3	0.87	8.63	0.096
80% CH_4 + 20% NH_3	0.82	8.57	0.205

mode was set to manual. The experimental apparatus is illustrated in Fig. 3.

A low-concentration aerosol generator (RBG 1000, Palas GmbH, Germany) was used to deliver pulverized coal into the flame. A cylindrical container was filled with the powder to be dispersed. The powder moved through the piston at a constant rate. The piston was controlled by an electric panel. Information about the aerosol generator was provided previously [27,38]. A subbituminous coal, Australian coal, was selected in our experiment due to its inherent advantages, such as high energy content, low sulfur and ash content, consistent quality, and accessibility. To offer a complete understanding of the coal used in this experiment, the *supplementary file* provides detailed information on the chemical and physical properties of the Australian coal, along with the proximate and elemental analyses. Additionally, Fig. 4 presents an SEM image that clearly depicts a compact surface of unburned pulverized coal.

4. Results and discussion

4.1. Coal hybrid combustion

As shown in Fig. 5**(a)-(c)**, pulverized coal which particle density was 48.26 g/m^3 was cofired with 100 %CH_4 + 0 %NH_3–air, 90 %CH_4 + 10 %NH_3–air, and 80 %CH_4 + 20 %NH_3–air, respectively. From the result, we know that the flame cone height tends to be longer while increasing the ratio of the NH_3 slightly. The flame cone is around 4-mm high in 0% NH_3 condition and then turns to 6-mm and 9-mm while the proportion increases from 10% to 20% of NH_3. The reason is that NH_3 reduced the flame propagation speed when CH_4 was partially replaced by NH_3. The flames were respectively bright blue and lavender, indicating the presence of NH_3.

Xia et al. [28] observed that before reacting, coal absorbs heat, and this leads to devolatilization of the char or some volatile matter, benefitting the combustion of the particles. The flame that was cofired with 20% NH_3 was the brightest, indicating that most of the particles would be burnt. Combustion was increased when the flame was cofired with NH_3 in the preliminary observation. However, NH_3-related pollutant emissions must be considered. The following section explores the use of two-color pyrometry to determine the cofiring temperature and the pollutants that may be produced.

4.2. Temperature as determined using two-color pyrometry

In two-color pyrometry, the wavelengths selected must be outside of

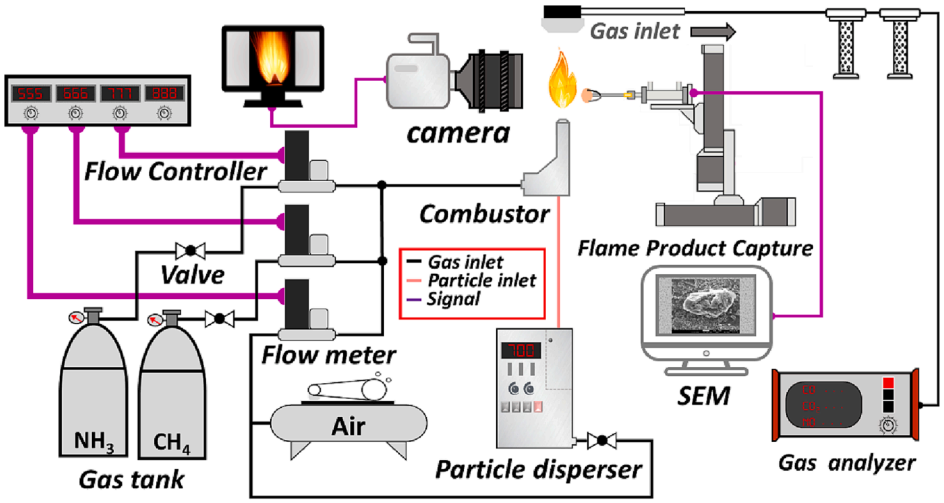

Fig. 3. Experimental apparatus.

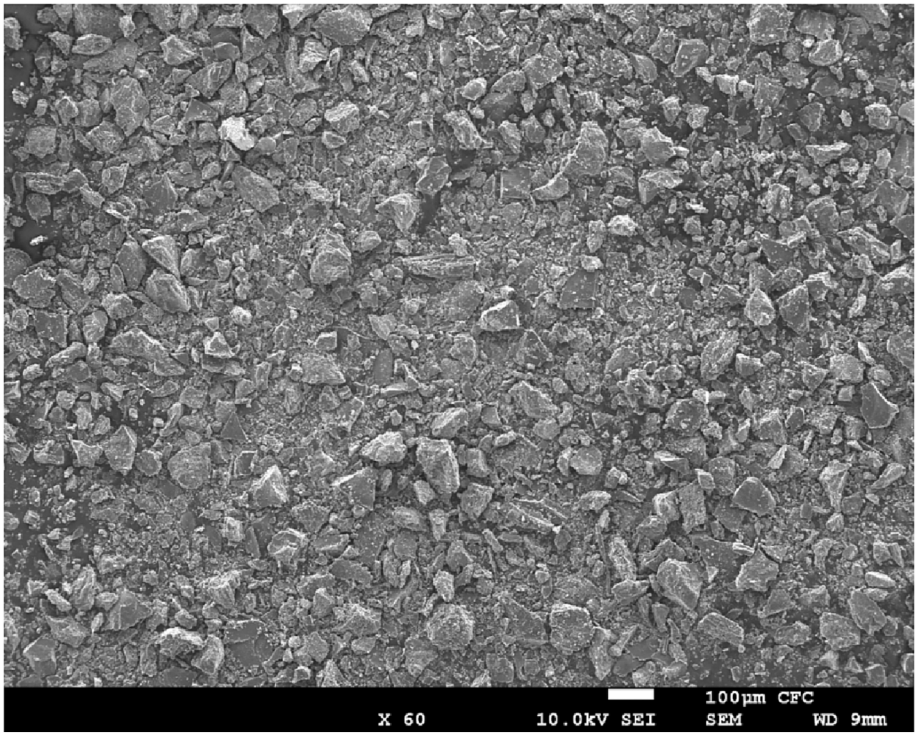

Fig. 4. SEM image of unburned pulverized coal.

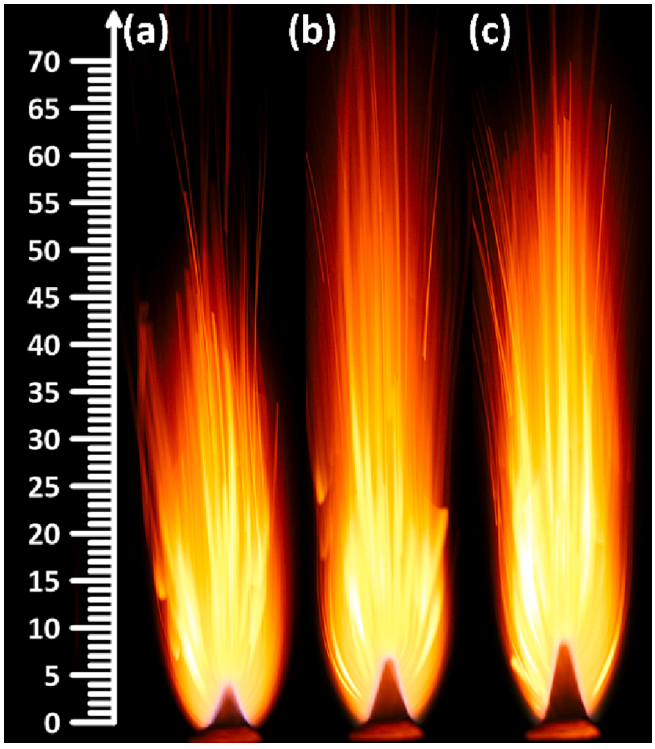

Fig. 5. Flames cofired with coal and (a) 100 %CH_4 + 0 %NH_3–air, (b) 90 %CH_4 + 10 %NH_3–air, and (c) 80 %CH_4 + 20 %NH_3–air.

the absorption wavelength zone of free radicals and gas molecules [21] such as CH (431.5 nm), OH (306 nm), and C_2 (516.5 nm). Three wavelength combinations were selected prior to the experimental trials: 550 and 690 nm, 550 and 750 nm, and 690 and 750 nm. The full width at half maximum of all wavelengths was set to 10 nm. The calibration curves are shown in Fig. 6. Excellent correction curves were obtained for the wavelength combinations 550 and 690 nm and 550 and 750 nm. The experimental temperature was increased from 1000 to 1150 K over intervals of 10 K. The solid squares, circles, and triangles in Fig. 6 represent the sample points. A relationship between the intensity and inverse of the temperature was obtained that could be used to calculate the dashed line through linear regression. According to the correction line, when the wavelengths were close to one another, a calibration error occurred in the 690-nm and 750-nm combination, leading to intersection of the two curves.

Two-color pyrometry was employed to examine the temperature profile at the centerline for each wavelength combination. Fig. 7 shows the temperature at the centerline. The temperature depends on the ratio of NH_3. The pulverized coal was cofired with a 100 %CH_4 + 0 %NH_3–air mixture, a 90 %CH_4 + 10 %NH_3–air mixture, and a 80 %CH_4 + 20 %NH_3–air mixture. The emissivity of soot particles was determined using an empirical formula. Due to a failure to detect soot particles in the flame cone, we set the original point at the top of the burner to 5 mm, indicating the location of the flame front. As the particles penetrated the flame sheet, they burnt and glowed, and images were captured with the CCD camera. The temperature for the 550-nm and 690-nm combination peaked at 1504 K for the condition without NH_3. The temperature tended to drop when particles were distant from the reaction surface. The temperature profiles were similar for each wavelength combination. However, the temperature was lower for the wavelength combinations in which the difference between the wavelengths was smaller. The temperature of the 690-nm and 750-nm combination was lower than that of the other combinations, regardless of the amount of NH_3 (0%, 10%, or 20% NH_3). Under these three conditions, temperature errors occurred if the two selected wavelengths were too close. The temperature measurements for two wavelength combinations under different ammonia contents are shown in Fig. 8, and the results are calculated by averaging 20 pieces of images. It should note that the 30-mm times 4-mm analyzed zone from the center of the burner outlet was selected and captured images by CCD camera. The temperature profiles are similar for each wavelength combination.

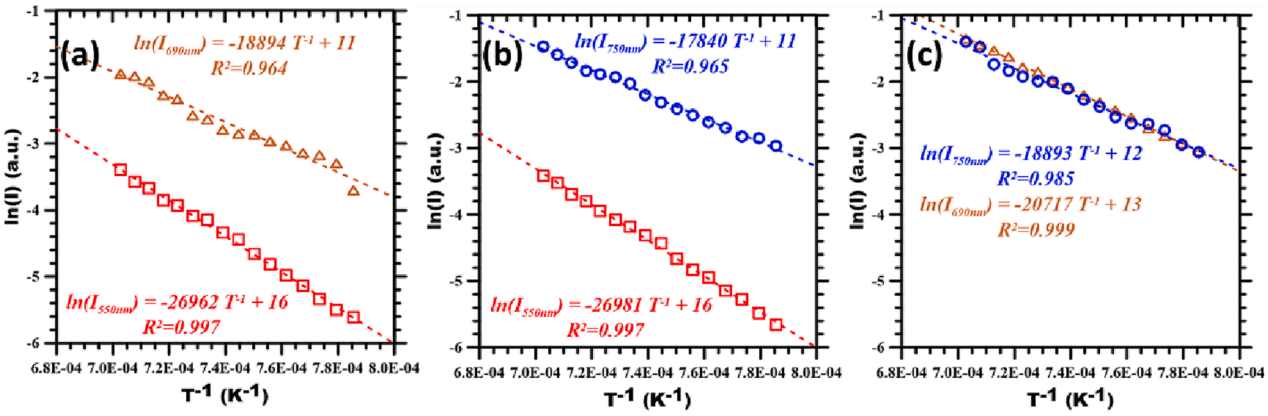

Fig. 6. Relationship between radiation intensity and apparent temperature for the wavelength combinations (a) 550 and 690 nm, (b) 550 and 750 nm, and (c) 690 and 750 nm.

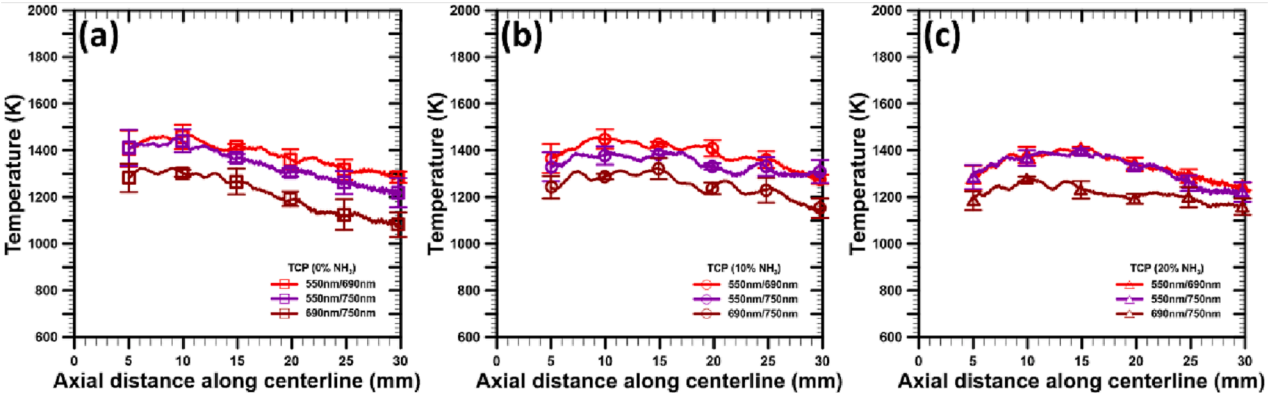

Fig. 7. Temperature according to two-color pyrometry at the centerline for each wavelength combination for (a) 0% NH_3, (b) 10% NH_3, and (c) 20% NH_3.

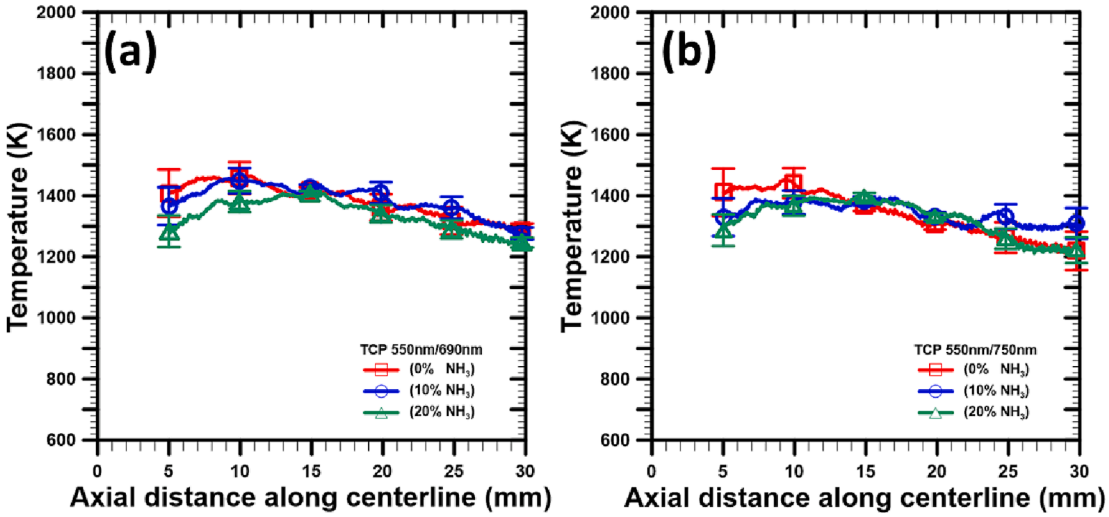

Fig. 8. Temperature profiles for each NH_3 ratio and the **(a)** 550-nm and 690-nm **(b)** and 550-nm and 750-nm wavelength combinations.

As the coal particles left the flame's surface, they immediately ignited and the temperature increased to 1500 K. When the particles had burnt out or left the primary reaction zone, the temperature decreased to 1300 K. Although the temperature profile was similar for each wavelength combination, the temperature of the 550-nm and 690-nm combination was higher than that of the 550-nm and 750-nm combination. Initially, the temperature decreased as the ratio of NH_3 was increased. The temperature slightly rose to 1450 K around 10 mm above the burner. Finally, the temperature curves of three different conditions start to overlap after 10-mm height of the flame. It means that the temperatures of the flame downstream under three different ammonia contents tend to stabilize. From these results indicated that the reaction of NH_3 in the flow field took longer than that of other substances, so the flame temperature under different ammonia replacement conditions

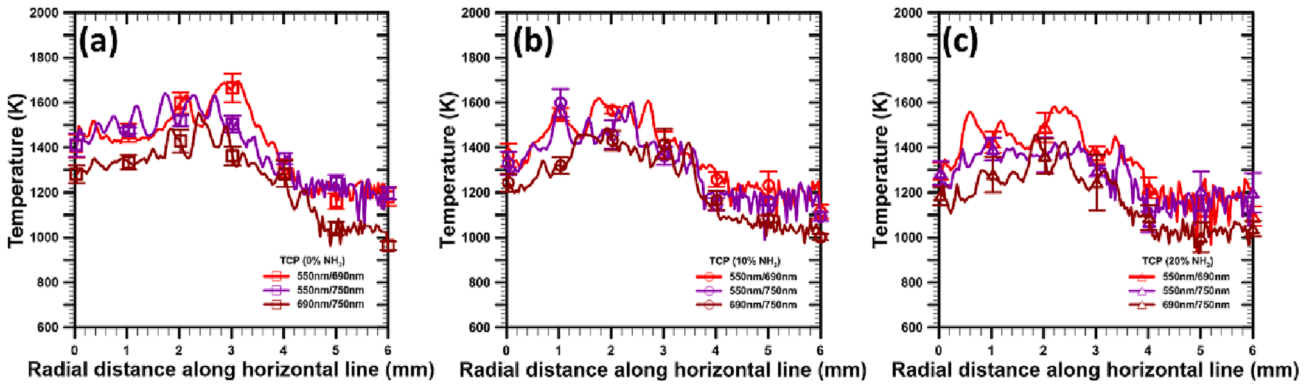

Fig. 9. Radial temperature at 5 mm under different wavelength combinations for **(a)** 0% NH_3, **(b)** 10% NH_3, and **(c)** 20% NH_3.

will be very close.

Coal particles are solid and disperseevenly in the axial and horizontal of the flame. Apart from the axial temperature,we determined the radial temperature distribution along a horizontal line. The radial temperature with different wavelength combinations is taken along the horizontal line at 5 mm and shown in Fig. 9**(a)–(c)**. The results show consistent temperature trends in the radial direction of the flame. It can be observed that the wavelength combination of 690–750 nm is lower than others. We can infer that the selected neighboring wavelengths led to inaccurate temperature calculations through the correlation line and this tendency.

Fig. 10 shows the radial temperature along horizontal lines at 5–30 mm heights.. The original point was the burner center, 6 mm from the outside. Particles 6 mm away from the radial burnt or drifted away. The curves in Fig. 10 show the same tendency in the distance to the central point for the various heights, resulting in temperature fluctuations until a maximum temperature was reached at 3 mm. Rough curves were obtained because the coal temperature detection was transient. An image had to be averaged before the temperature could be calculated. Therefore, the concentration of particles was low in some areas. The images were averaged at least 20 times in this study. Temperatures were higher at the radial line than at the central line.

At 5 mm from the center for the 20% NH_3 mixture, the temperature oscillated in the region of 4–6 mm. This NH_3 ratio yielded a dilute or disengaged response. As the flow field gradually reacted downstream, the effect of NH_3 on the radial temperature profile weakened progressively until the profile matched the 0% NH_3 temperature profile. The trends in the temperature distributions were similar for the two wavelength combinations. The 550-nm and 690-nm combination resulted in higher temperature than did the 550-nm and 750-nm combination. The reaction of NH_3 was diminished downstream of the flow field, probably because saturation was reached under these conditions, leading to the same distribution without further replacement.

To determine the global flame temperature profile, we used a probability density function. By taking the 550-nm and 690-nm wavelength combination at different NH_3 ratios as an example (Fig. 11), we discovered that the temperature in the high region of the reaction zone decreased when the NH_3 ratio was increased from 0% to 10%, bringing the temperature closer to the normal distribution. Table 2 shows the average temperature, average higher temperature, and standard deviation values, where the high temperature is the average of the temperature values in the 80th percentile of all temperature values (i.e., the 20% highest temperatures).

4.3. Comparison of gaseous flame temperatures

A R-type thermocouple was used to measure the effect of NH_3 on the flame temperature with the increase of the flame height because the gas phase temperature of the cofiring was unknown. The temperature was calibrated using thermal radiation as proposed by Basem and Yunus [29,30]. The corrected equation is as follows:

$$T = T_{TC} + \frac{\varepsilon\sigma d_{TC}(T_{TC}^4 - T_{surr}^4)}{kNu} \tag{11}$$

where Nu is the Nusselt number, T is the correction temperature (K), T_{TC} is the thermocouple temperature (K), T_{surr} is the ambient temperature (K), d_{TC} is the diameter of the thermocouple bead (m), ε is the emission of the thermocouple bead, k is the thermal conductivity of hot gases (W/mK), and σ is the Stefan–Boltzmann constant (5.67×10^{-8} W/m^2K^4).

The correction temperature result is shown in Fig. 12. The effect of NH_3 was significant at 10 mm above the burner, and the temperature curves overlapped while coal continued to burn downstream of the flame.However, the temperature decreased at the original point when coal was added because the coal particles absorbed the heat of the flame. The temperature of the flame cofired with coal and NH_3 changed considerably, especially for the 20% NH_3 ratio.

The pulverized coal first absorbed the heat which led to a relatively low temperature. The same thing happened with the addition of NH_3. Due to the low reactivity of NH_3, the reaction took time after the addition of pulverized coal, leading to a slow temperature increase. The temperature increase was slowest for the 20% NH_3 mixture. It could be noted that two-color pyrometry only could capture the particle temperature. It caused we got different values of temperature between two-color pyrometry and thermocouple. The overall trend of these two methodologies was similar even though the value was different. Therefore, the global temperature variation could be deduced based on the temperature trend.

In addition, the adiabatic flame temperature was calculated using CHEMIN-PRO software. The tendency of the adiabatic flame temperature under the different proportions of ammonia is also identical to our experiment. The amount of NH_3 in the gas mixtures ranged from 0% to 50%. The adiabatic flame temperature decreased as the amount of NH_3 was increased. This result was similar to that obtained using two-color pyrometry.

4.4. Emission of CO and NO_X pollutants

The incomplete combustion of NH_3 produces various pollutants, among which NO_X is the most notorious. Cofiring with NH_3 led to increased production of NO_X·NH_3 may be reduced and exothermically generate heat and CO is generated through the combustion process of devolatilization, pyrolysis, etc. Insufficient data were available regarding the CO production rate when NH_3 was added. This study measured pollutant emissions to gain an understanding of the cofiring mechanism, as shown in Figs. 13 and 14. A comparison of pollution generation was made between the cases with and without coal combustion. The sign of the red dot represents pure CH_4–air combustion under stoichiometric conditions. According to the results, when pure

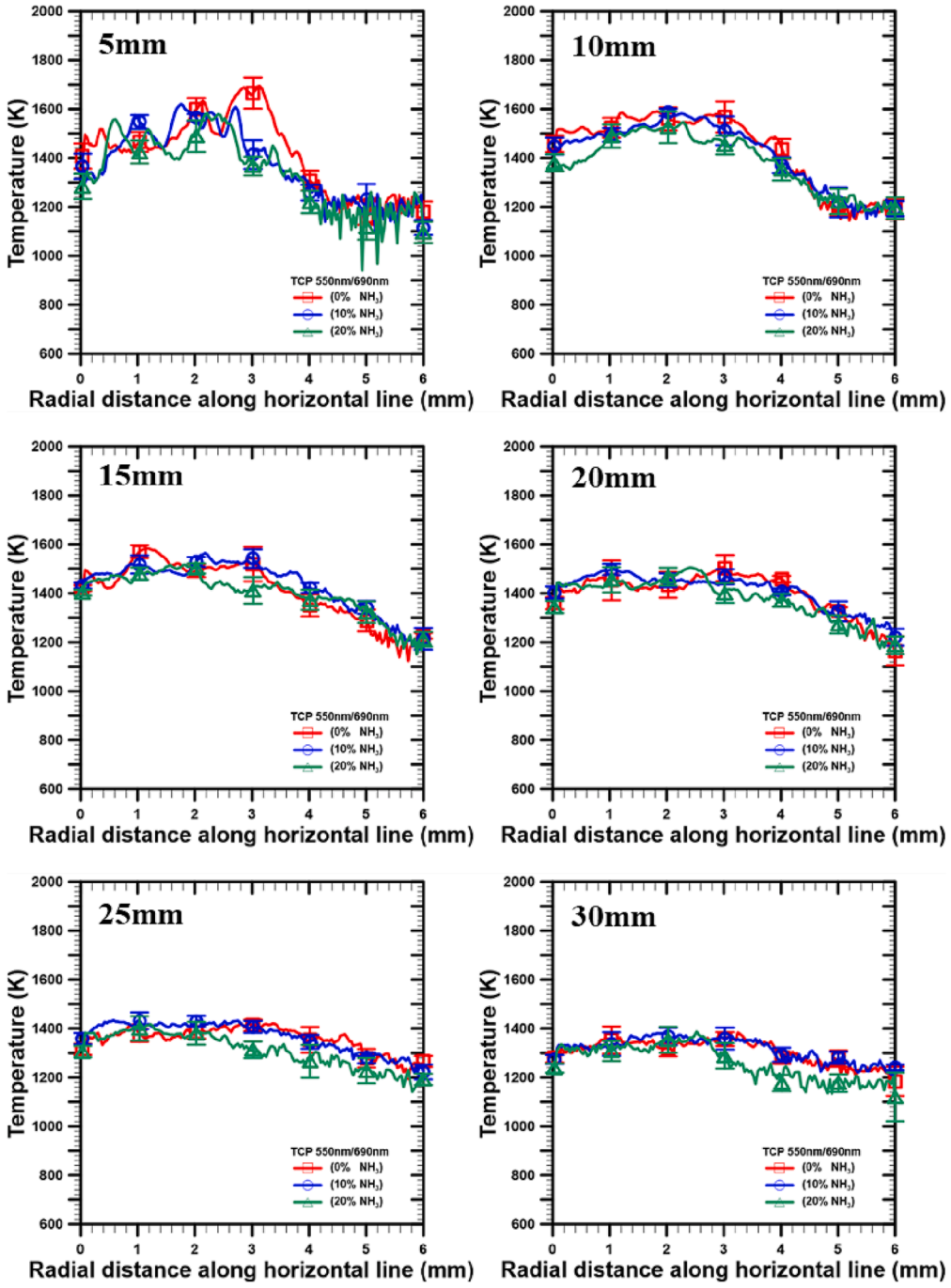

Fig. 10. Radial temperature of different NH_3 ratios along horizontal lines with various heights for the 550-nm and 690-nm wavelength combination.

CH_4–air combustion is conducted without adding coal particles, the CO emission concentration is 50.90 ppm. However, when coal particle feeding rates increase, specifically at rates of 0.24, 0.48, and 0.72 g/min, the CO concentration rises to 539.63, 495.09, and 491.87 ppm, respectively. This is due to the pyrolysis of pulverized coal after absorbing heat, resulting in higher CO emissions when coal particles are involved in the combustion process. Notably, there is only minimal variation in CO concentration after 0.24 g/min, owing to the finite pyrolysis of the particles leading to a limited increase in pollutant concentrations.

It is noteworthy that in the case of ammonia-methane co-combustion, the addition of coal particles results in a remarkable reduction of CO concentration. For instance, when considering the 90 %CH_4 + 10 % NH_3 mixture and adjusting the coal particle feeding rate from 0 g/min to 0.24 g/min, the CO concentration drops from the initial 1160.92 ppm to 930.73 ppm. Moreover, under the condition of 80 %CH_4 + 20 % NH_3–air, the CO concentration decreases by approximately 34%. This phenomenon is attributed to experimental and numerical studies conducted by [32] to elucidate the cofiring process.

$$soot + NO \rightarrow 0.994soot + 0.5N_2 + CO \quad (12)$$

$$H_2O + CO \rightarrow H_2 + CO_2 \quad (13)$$

The combustion of NH_3 results in the production of NO_X, which can react with soot particles generated during the pyrolysis of pulverized coal. Such a reaction may lead to the formation of carbon monoxide. However, the addition of H_2O in NH_3 during coal–NH_3 co-firing caused a reduction in CO concentration. This is attributed to the fact that CO

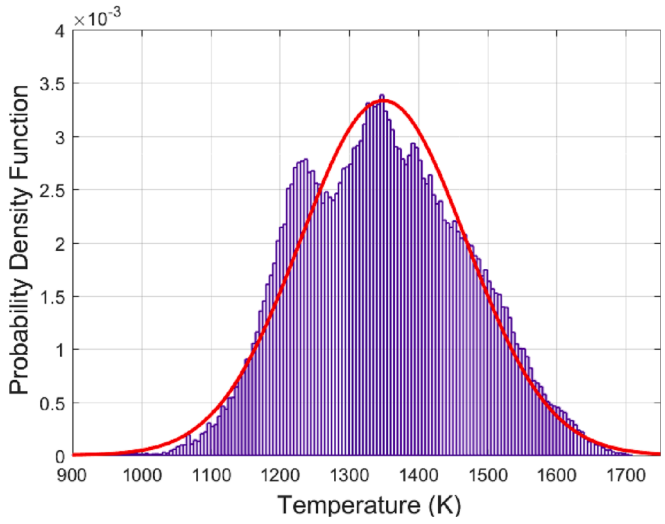

Fig. 11. Correlation between temperature and the probability density function in the absence of NH_3 for the 550-nm and 690-nm wavelength combination.

Table 2
Temperature parameters for different NH_3 ratios and wavelength combinations.

NH_3		550 nm/690 nm	550 nm/750 nm	690 nm/750 nm
0%	*Median(K)*	1349.5	1312.8	1184.8
	Standard Deviation(K)	119.5	122.8	125.6
	Average higher temperature (K)	1670.4	1637.4	1505.9
10%	*Median(K)*	1351.4	1310.9	1214.4
	Standard Deviation(K)	109.37	106.5	114.9
	Average higher temperature (K)	1666.5	1605.6	1578.4
20%	*Median(K)*	1318.8	1294.2	1178.3
	Standard Deviation(K)	112.9	112.2	112.4
	Average higher temperature (K)	1641.5	1617.6	1533.6

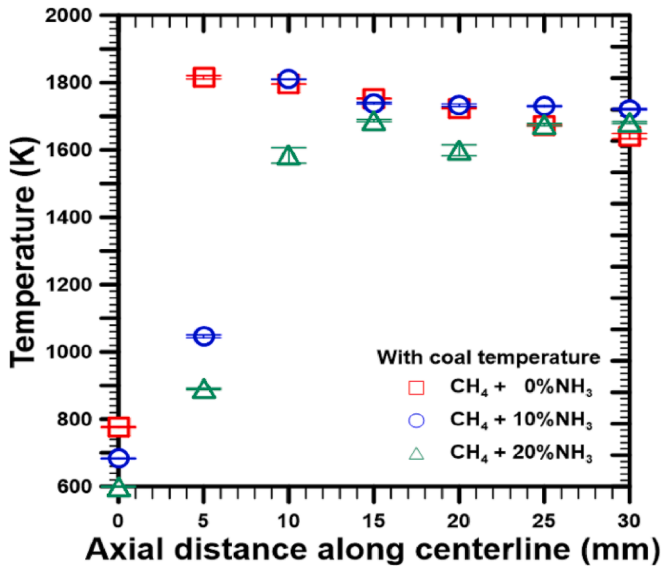

Fig. 12. Temperature at the axial centerline with coal.

reacts readily with H_2O, which can lead to a decrease in CO emissions. Our findings are consistent with those of a study conducted by Ishihara et al. [32], which reported a significant reduction in CO emissions (by

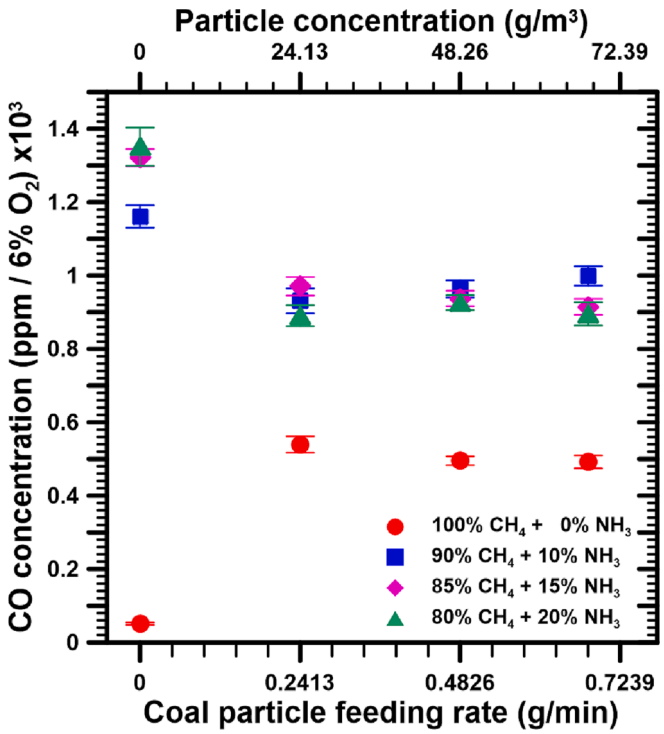

Fig. 13. Correlation between coal feeding rate and CO emission.

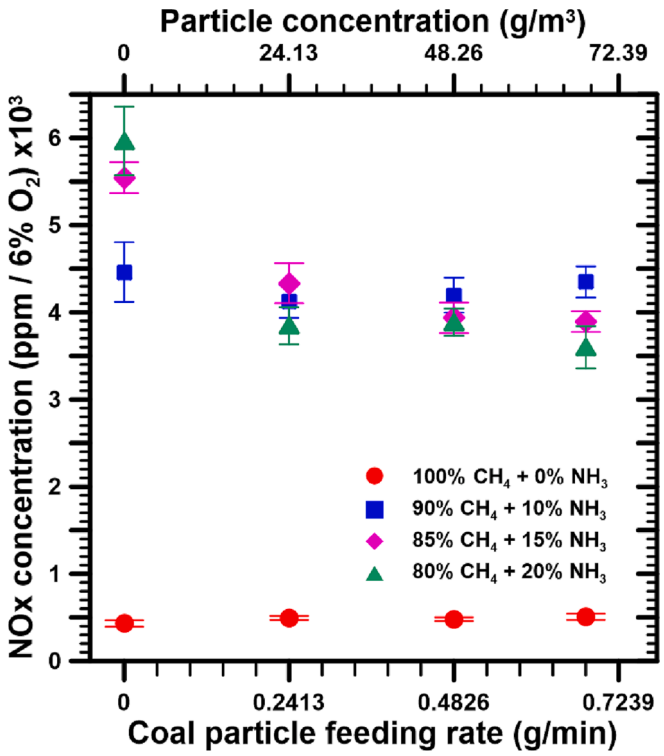

Fig. 14. Correlation between coal feeding rate and NO_X emission.

0.7 to 0.9 times) due to NH_3 co-firing, highlighting the effectiveness of this technique.

On the contrary, the addition of ammonia leads to an increase in CO concentration due to the fact that NH_3 requires more air compared to CH_4. If there is insufficient oxygen supply, it can result in an increase in CO emissions. Li et al. observed the same results that the temperature

decreases and CO emissions increase when NH_3 is added to a combustion process [31].

The correlation between the coal feeding rate and NO_X emission is illustrated in Fig. 14. The results show that under pure CH_4–air combustion without the addition of coal particles, the NOx emission concentration is 431.25 ppm. However, with an increase in coal particle feeding rate, the concentration of NOx remains almost the same. Coal did not significantly affect NO_X emissions under conditions of pure CH_4–air. The addition of NH_3 resulted in a significant increase in the amount of NOx. Specifically, under ammonia substitution proportions ranging from 10% to 20%, the NOx concentrations increased to 4461.51, 5543.68, and 5965.73 ppm, respectively. Ideally, the combustion of NH_3 would produce N_2 and H_2O without producing NO_X. However, in a typical environment, NO_X is emitted. The emission of NO_X is one of the challenges encountered in NH_3 combustion. Studies have investigated methods of decreasing NO_X emissions when cofiring pulverized coal with NH_3 [33], such as by forming char after heating and devolatilization of coal. The combustion of NH_3 leads to the decomposition of NH_3 into NO_X, which could react with carbon to reduce the final amount of NO_X. The reaction process is as follows:

$$2NO + C(char) \rightarrow N_2 + O_2 + C(char) \quad (14)$$

This study also observed a similar trend under CH_4–NH_3–air co-combustion conditions. Increasing the coal particle feeding rate at rates of 0.24, 0.48, and 0.72 g/min had a noticeable impact on NOx emissions. For example, in the case of 90 %CH_4 + 10 %NH_3–air, adjusting the coal particle feeding rate from 0 to 0.24 g/min resulted in a decrease in NOx concentration from 4461.51 ppm to 4124.60 ppm. Notably, in the 80 %CH_4 + 20 %NH_3–air condition, there was a significant reduction of approximately 35% in NOx emissions. These results further demonstrate that the addition of ammonia has a significant beneficial effect on coal combustion.

4.5. Morphology of pulverized coal

Four heights above the burner (5, 10, 20, and 35 mm) were selected to investigate the transformation of coal in a flame. Coal particles were collected using a copper-plated clip with a 0.2-mm-tip and self-locking tweezers. Fig. 15 depicts the transformation of coal for its combustion with or without NH_3 at various heights. When particles were present in the flame cone, smaller particles were pyrolyzed and had a similar appearance to unburned particles. At greater height, the coal particles were smaller. Three conditions led to the same result but differing numbers of fractures on the surface of the coal particles, which was mainly due to the formation of char after coal heating and devolatilization. The process of devolatilization or pyrolysis occurred on the coal's surface; therefore, the volatile particles may have been burnt with the decomposed NH_3, causing irregular cracks on the surface. The binarization method was used to calculate the area of the coal particles after combustion. The binarization method involves creating a binary image from a 2D or 3D grayscale image, replacing all values above a globally determined threshold (1), and setting all other values to 0 [34]. A schematic of the binarization method is displayed in Fig. 16.

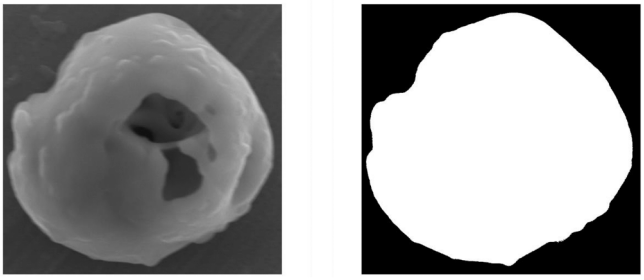

Fig. 16. Binarization method schematic.

In binarization, the correlation between a pixel and the actual size must be calculated first. The size can then be obtained by approximating the area of the circle. A method of an analysis of circle approximation will be utilized in this study. Fig. 17 shows the particle projected area of the circle at various heights. For each condition, calculations were performed with at least 15 particles. Unfortunately, few particles were captured at locations higher than 25 mm because the particles shrank after being burnt. Table 3 indicates the projected area and density of the coal particles captured by the tiny copper plate. The copper plate had an area of 3×10^{-6} m^2. In the CH_4–air flame, the particle shrinking rate, defined as the percentage decline in the particles' projected area from that at the previously observed location, was 54.4%, 82.1%, and 75.1% at heights of 10, 20, and 35 mm, respectively. The particle shrinking rates were similar in the CH_4–NH_3 10% and CH_4–NH_3 20% flames. The particles' projected areas at heights of 10 mm and above for the CH_4–NH_3 10% and CH_4–NH_3 20% flames were smaller than those for the CH_4–NH_3 0% flame. These findings indicate that addition of NH_3 to the CH_4–air flame promotes coal combustion. The particle density was 22.7, 19, 11, and 5.6 g/m^3 at 5, 10, 20, and 35 mm, respectively, indicating that the particle density decreased with increasing height. Many coal particles were burnt·NH_3 promoted the complete combustion of coal because decomposing NH_3 reacted with coal and char. CO and NH_3 both will react with coal in combustion.

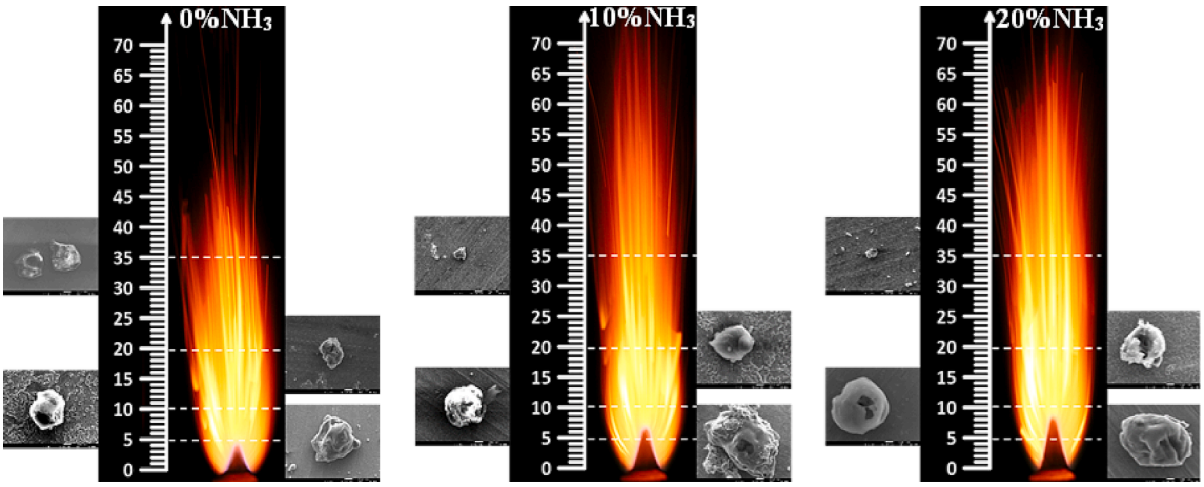

Fig. 15. Transformation of pulverized coal particles of different sizes at various positions.

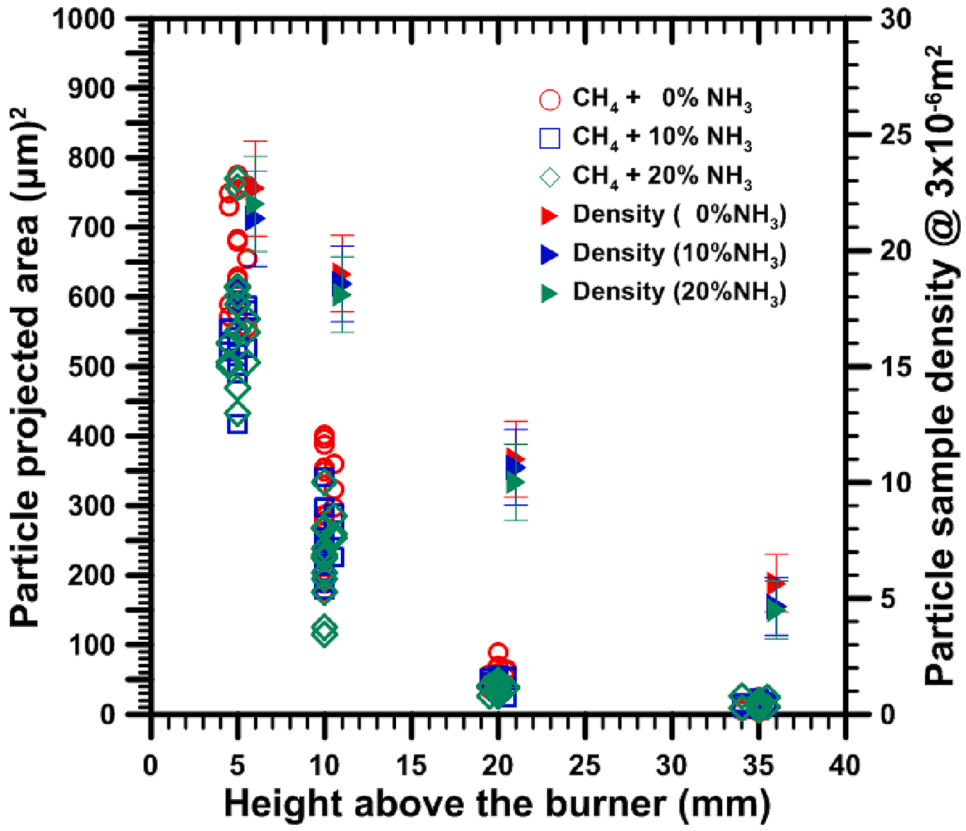

Fig. 17. Particle projected area at various heights.

Table 3
Projected area and density of coal particles captured at various heights.

Fuel condition	Particle projected area (μm^2) Height = 5 mm	10 mm	20 mm	35 mm
100 %CH_4 + 0 % NH_3	656.5 ± 78.17	299.27 ± 78.00	53.63 ± 15.04	13.33 ± 7.00
90 %CH_4 + 10 % NH_3	546.8 ± 52.97	241.07 ± 43.89	42.86 ± 8.76	14.70 ± 4.81
80 %CH_4 + 20 % NH_3	571.00 ± 94.12	226.87 ± 57.94	37.43 ± 7.36	14.91 ± 6.27
	Particle sampling density @ 3 × 10^{-6} m^2 of a copper plate			
100 %CH_4 + 0 % NH_3	22.7 ± 2.05	19.0 ± 1.63	11.0 ± 1.63	5.6 ± 1.25
90 %CH_4 + 10 % NH_3	21.4 ± 2.05	18.5 ± 1.63	10.6 ± 1.63	4.7 ± 1.25
80 %CH_4 + 20 % NH_3	22.0 ± 2.05	18.1 ± 1.63	10.0 ± 1.63	4.5 ± 1.25

5. Conclusions

The study of NH_3-CH_4-air co-combustion with pulverized coal has provided insights into the cofiring mechanism and its impact on pollutant emissions. The findings revealed that incomplete combustion of NH_3 − CH_4 mixture leads to the generation of different pollutants. In the absence of coal particles, increasing the ammonia content from 0% to 20% resulted in a significant increase in CO concentration from 50.90 to 1351.05 ppm. Similarly, the concentration of NOx rose from 431.25 to 5965.73 ppm. The addition of coal particles in pure CH_4-air combustion resulted in a significant increase in CO emissions, primarily attributed to the pyrolysis of pulverized coal. Specifically, when the feeding rate was increased from 0 to 0.24 g/min, the CO concentration showed a substantial rise from 50.90 ppm to 539.63 ppm. In contrast, the effect on NOx emissions was found to be minimal or insignificant.

Interestingly, the co-combustion of NH_3-CH_4-air with coal particles, the addition of coal particles led to a significant decrease in CO and NOx concentration. CO emissions decrease when NH_3 is cofired with coal, possibly due to reactions between NOx and soot particles, as well as increased presence of H_2O, which facilitates CO conversion to CO_2. Significantly, the co-combustion of NH_3 with coal resulted in a substantial reduction of approximately 34% in CO emissions under 80 % CH_4 + 20 %NH_3 − air condition.

In terms of NOx emissions, there was a significant decrease of approximately 35%. The reduction of NOx emissions can be attributed to the reaction between NO and char produced by NH_3 − coal combustion, which in turn inhibits the formation of NOx. These results contribute to the understanding of cofiring mechanisms and provide valuable insights for mitigating pollutant emissions in coal-NH_3 co-combustion systems.

In the end of the study, it was observed that the addition of NH_3 to the CH_4 − air flame promoted coal combustion and resulted in significant changes in the characteristics of the coal particles. At different heights above the burner, the coal particles underwent transformation during combustion. The binarization method was used to analyze the area of the coal particles after combustion. It was found that the particle shrinking rate increased with the increase in height, indicating that the particles experienced significant reduction in their projected area. The addition of NH_3, at both 10% and 20% concentrations, further decreased the particles projected areas compared to the CH_4 − air flame without NH_3. This suggests that NH_3 promoted the complete combustion of coal by reacting with both coal and char. Furthermore, the particle density decreased with increasing height, indicating that many coal particles were burnt during combustion. The presence of NH_3 contributed to the complete combustion of coal by reacting with coal and char, further supporting the findings of improved coal combustion in the presence of NH_3.

These results indicate that introducing NH_3 into the CH_4-air flame had a beneficial effect on coal combustion. It led to an improved coal consumption rate, facilitating the complete combustion of coal and reduction of the pollutant. These observations underscore the potential of NH_3 cofiring as a promising approach to enhance the overall combustion efficiency of coal.

CRediT authorship contribution statement

Yueh-Heng Li: Conceptualization, Funding acquisition, Investigation, Project administration, Writing – original draft, Writing – review & editing. **Bo-Cheng Chuang:** Data curation, Investigation, Validation, Writing – original draft. **Po-Hung Lin:** Investigation, Validation, Writing – review & editing. **Janusz Lasek:** Funding acquisition, Project administration.

Declaration of Competing Interest

The authors declare that they have no known competing financial interests or personal relationships that could have appeared to influence the work reported in this paper.

Data availability

Data will be made available on request.

Acknowledgments

This work was financially supported by the National Science and Technology Council (NSTC, Taiwan) and National Center for Research and Development (NCBR, Poland) under the grant number NSTC 112-2923-E-006-002-MY3.

Appendix A. Supplementary data

Supplementary data to this article can be found online at https://doi.org/10.1016/j.fuel.2023.128825.

References

[1] Pratt DT, Smoot L, Pratt D. Pulverized coal combustion and gasification: Springer; 1979.
[2] Zakeri B, Syri S, Rinne S. Higher renewable energy integration into the existing energy system of Finland – Is there any maximum limit? Energy 2015;92:244–59.
[3] Jacobson MZ, Delucchi MA. Providing all global energy with wind, water, and solar power, Part I: Technologies, energy resources, quantities and areas of infrastructure, and materials. Energy Policy 2011;39:1154–69.
[4] Nakata T, Silva D, Rodionov M. Application of energy system models for designing a low-carbon society. Fuel Energy Abstracts 2011.
[5] Cavazos Guerra C, Lauer A, Rosenthal E. Clean Air and White Ice: Governing Black Carbon Emissions Affecting the Arctic. 2017. p. 231-56.
[6] Solomon PR, Fletcher TH. Impact of coal pyrolysis on combustion. Symposium (International) on combustion: Elsevier; 1994. p. 463-74.
[7] Williams A, Backreedy R, Habib R, Jones J, Pourkashanian M. Modelling coal combustion: the current position. Fuel 2002;81:605–18.
[8] Yu J, Lucas JA, Wall TF. Formation of the structure of chars during devolatilization of pulverized coal and its thermoproperties: A review. Prog Energy Combust Sci 2007;33:135–70.
[9] Saxena S, Jotshi C. Fluidized-bed incineration of waste materials. Prog Energy Combust Sci 1994;20:281–324.
[10] Benfell KE, Liu G, Roberts D, Harris DJ, Lucas J, Bailey JG, et al. Modeling char combustion: The influence of parent coal petrography and pyrolysis pressure on the structure and intrinsic reactivity of its char2000.
[11] Wall T, Tate A, Bailey J, Jenness L, Mitchell R, Hurt R. The temperature, burning rates and char character of pulverised coal particles prepared from maceral concentrates. Symposium (International) on Combustion: Elsevier; 1992. p. 1207-15.
[12] Wall T, Liu G, Wu H-w, Roberts D, Benfell K, Gupta S, et al. The effects of pressure on coal reactions during pulverised coal combustion and gasification. Prog Energy Combust Sci 2002;5:405–33.
[13] Wall TF, Yu J, Wu H, Liu G, Lucas JA, Harris D. Effects of pressure on ash formation during pulverized coal combustion and gasification. Preprints of Symposia—American Chemical Society, Division of Fuel Chemistry: Citeseer; 2002. p. 801-06.
[14] Essenhigh RH, Misra MK, Shaw DW. Ignition of coal particles: a review. Combust Flame 1989;77:3–30.
[15] Adeosun A, Huang Q, Li T, Gopan A, Wang X, Li S, et al. Characterization of a new Hencken burner with a transition from a reducing-to-oxidizing environment for fundamental coal studies. Rev Sci Instrum 2018;89.
[16] Du X, Annamalai K. The transient ignition of isolated coal particle. Combust Flame 1994;97:339–54.
[17] Annamalai K, Durbetaki P. A theory on transition of ignition phase of coal particles. Combust Flame 1977;29:193–208.
[18] Valera-Medina A, Amer-Hatem F, Azad A, Dedoussi I, De Joannon M, Fernandes R, et al. Review on ammonia as a potential fuel: from synthesis to economics. Energy Fuel 2021;35:6964–7029.
[19] Lee H, Lee M-J. Recent Advances in Ammonia Combustion Technology in Thermal Power Generation System for Carbon Emission Reduction. Energies 2021;14:5604.
[20] Hottel HC, Broughton FP. Determination of true temperature and total radiation from luminous gas flames. Ind Eng Chem Anal Ed 1932;4:166–75.
[21] Zhao H, Ladommatos N. Optical diagnostics for soot and temperature measurement in diesel engines. Prog Energy Combust Sci 1998;24:221–55.
[22] Lafolletie RM, Hedman PO, Smith PJ. An analysis of coal particle temperature measurements with two-color optical pyrometers. Combust Sci Technol 1989;66:93–105.
[23] Matsui Y, Kamimoto T, Matsuoka S. Formation and oxidation processes of soot particulates in a DI diesel engine-an experimental study via the two-color method. SAE Trans 1982, 1923–35..
[24] Reggeti S, Agrawal A, Bittle J. Two-color pyrometry system to eliminate optical errors for spatially resolved measurements in flames. Appl Opt 2019;58:8905.
[25] Bradley D, Matthews KJ. Measurement of High Gas Temperatures with Fine Wire Thermocouples. J Mech Eng Sci 1968;10:299–305.
[26] Rocha RC, Ramos CF, Costa M, Bai X-S. Combustion of NH3/CH4/Air and NH3/H2/Air Mixtures in a Porous Burner: Experiments and Kinetic Modeling. Energy Fuel 2019;33:12767–80.
[27] Li Y-H, Pangestu S, Purwanto A, Chen C-T. Synergetic combustion behavior of aluminum and coal addition in hybrid iron-methane-air premixed flames. Combust Flame 2021;228:364–74.
[28] Xia Y, Hadi K, Hashimoto G, Hashimoto N, Fujita O. Effect of ammonia/oxygen/nitrogen equivalence ratio on spherical turbulent flame propagation of pulverized coal/ammonia co-combustion. Proc Combust Inst 2021;38:4043–52.
[29] Rabee BA. The effect of inverse diffusion flame burner-diameter on flame characteristics and emissions. Energy 2018;160:1201–7.
[30] Çengel YA. Heat Transfer: A Practical Approach. McGraw-Hill; 2003.
[31] Li J, Lai S, Chen D, Wu R, Kobayashi N, Deng L, et al. A review on combustion characteristics of ammonia as a carbon-free fuel. Front Energy Res 2021;9.
[32] Ishihara S, Zhang J, Ito T. Numerical calculation with detailed chemistry of effect of ammonia co-firing on NO emissions in a coal-fired boiler. Fuel 2020;266.
[33] Tsukada N, Kinoshita N, Kabuki Y, Taguchi Y, Takashima Y, Tsumura T, et al. Role of OH Radical in Fuel-NOx Formation during Cocombustion of Ammonia with Hydrogen, Methane, Coal, and Biomass. Energy Fuel 2020;34:4777–87.
[34] Otsu N. A threshold selection method from gray level histograms. IEEE Trans Syst Man Cybern 1979;9:62–6.
[35] Li Y-H, Chen G-B, Lin Y-C, Chao Y-C. Effects of flue gas recirculation on the premixed oxy-methane flames in atmospheric condition. Energy 2015;89:845–57.
[36] Kuo W.-C.m Lasek J, Słowik K, Głód K, Jagustyn B, Li Y-H, Cygan A. Low-temperature pre-treatment of municipal solid waste for efficient application in combustion systems. Energy Conversion and Management 2019;196:525–35.
[37] Li Y-H, Hsu C-H, Lin P-H, Chen C-H. Thermal effect and oxygen-enriched effect of N_2O decomposition on soot formation in ethylene diffusion flames. Fuel 2022;329:125430.
[38] Li Y-H, Purwanto A, Chuang B-C. Micro-explosion mechanism of iron hybrid methane-air premixed flames. Fuel 2022;325:1124841.
[39] Li Y-H, Reddy SK, Chen C-H. Effects of the nitrous oxide decomposition reaction on soot precursors in nitrous oxide/ethylene diffusion flames. Energy 2021;235:121364.
[40] Huang C-W, Li Y-H, Xiao K-L, Lasek J. Cofiring characteristics of coal blended with torrefied Miscanthus Biochar optimized with three Taguchi indexes. Energy 2019;172:566–79.
[41] Li Y-H, Lin H-T, Xiao K-L, Lasek J. Combustion behavior of coal pellets blended with Miscanthus biochar. Energy 2018;163:180–90.
[42] Chen C-H, Li Y-H. Role of N_2O formation of methane/nitrous oxide premixed flames. Combustion and Flame 2021;223:42–54.
[43] Li Y-H, Liang J-W, Lin H-J. Development of laminar burning velocity measurement system in premixed flames with hydrogen-content syngas or strong oxidizer conditions in a slot burner. Case Studies in Thermal Engineering 2022;35:102162.
[44] Li Y-H, Chen H-H. Analysis of syngas production rate in empty fruit bunch steam gasification with varying control factors. International Journal of Hydrogen Energy 2018;43(2):667–75.
[45] Chai WS, Bao Y, Jin P, Tang G, Zhou L. A review on ammonia, ammonia-hydrogen and ammonia-methane fuels. Renewable and Sustainable Energy Reviews 2021;147:111254.